JOURNAL OF MATERIALS SCIENCE **38** (2003) 4183–4191

The mechanical properties related to the dominant microstructure in the weld zone of dissimilar formed Al alloy joints by friction stir welding

W. B. LEE
Department of Advanced Materials Engineering, Sungkyunkwan University, 300 Choencheon-dong, Jangan-gu, Suwon, Kyounggi-do 440-746, Korea

Y. M. YEON
Department of Automated System, Suwon-Science College, Suwon, Korea

S. B. JUNG*
Department of Advanced Materials Engineering, Sungkyunkwan University, 300 Choencheon-dong, Jangan-gu, Suwon, Kyounggi-do 440-746, Korea
E-mail: sbjung@skku.ac.kr

The joint properties of dissimilar formed Al alloys, cast Al alloy and wrought Al alloy, were examined with various welding conditions. Friction stir welding method could be applied to join dissimilar formed Al alloys which had different mechanical properties without weld zone defects under wide range of welding condition.

The weld zone of dissimilar formed Al alloy exhibited the complex structure of the two materials and mainly composed of the retreating side material.

The mechanical properties also depended on the dominant microstructure of the weld zone with welding conditions. The different mechanical properties of the weld zone with welding conditions were related to the behavior of the precipitates of wrought Al alloy and Si particles of cast Al alloy. The higher mechanical properties of the weld zone were acquired when a relatively harder material, wrought Al alloy, was fixed at the retreating side.

1. Introduction

Generally, Al alloys have many specific properties and can be applied to many structural parts that need both light weight and high mechanical properties. In these days, Al alloys have been used in the transportation industry such as high speed rail way [1], shipping [2] and external fuel tanks of rockets [3]. Structural parts and frames composed of Al alloys must be welded using the sound welding technique commonly employed in this industry. If Al alloys were welded using conventional fusion welding, many welding defects, such as voids, hot cracking and distortion, related to the melting and solidification were formed in the weld zone. Moreover, problems of fusion welded Al alloys were the precipitates resolution, the loss of work hardening effect and hard to melt for welding [4–7]. Therefore, the solid state bonding technique is highly recommended to solve these many problems. Friction stir welding, invented by TWI in 1991, is a promising technique because it resulted in superior joint quality of the varieties of Al alloys [8].

Many researches about FSW Al alloys have been conducted since the FSW applied to join the variety of Al alloys. Main subjects were classified as the microstructure inspection related to the mechanical properties [9–12], friction stir welding mechanism of the weld zone formation and the materials flow phenomena using marker insert technique [13, 14] and the prediction of the weld zone's residual stress, the heat flow and the temperature by simulation method [15, 16].

Recently, the aspect of industrial structures has become more complicated, making the joining method of the dissimilar materials an indispensable technique. Very few cases of dissimilar materials joined by friction welding method have been presented. Some examples are 2024/6061 [17], 6061/copper [18] and 6N01/5083 [19], which revealed the complex microstructural behaviors.

In this present study, dissimilar formed Al alloys were joined by friction stir welding method with various welding conditions. The objective of present research is to evaluate the microstructure and mechanical

*Author to whom all correspondence should be addressed.

TABLE I Chemical compositions of each material

	Si	Fe	Cu	Mn	Mg	Cr	Ni	Zn	Ti	Sn	Al
A356	7.006	0.136	0.096	0.002	0.25	0.008	0.007	0.05	0.154	0.004	Bal
6061	0.567	0.173	0.212	0.031	0.92	0.066	–	0.021	0.018	–	Bal

properties with the fixed location of each material and friction stir welding speed.

2. Experimental procedure

The materials used in this study were cast A356 Al alloy and wrought 6061 Al alloy which had 140 mm in length, 70 mm in width and 4 mm in thickness. Microstructure of cast A356 Al alloy was composed of Al solid solution (α) and the Al-Si eutectic structure. Wrought 6061 Al alloy is the one of precipitation hardening Al alloys by the aging process at an adequate temperature and time. Chemical compositions of each material are displayed in Table I.

Fig. 1 illustrates the nomenclature of each weld zone. Each side of the weld zone can be divided into the retreating side and the advancing side with the relation between tool rotation directions and welding direction.

The welding conditions were divided into the condition A and condition B for convenience. Condition A identified the A356 Al alloys fixed at the retreating side and 6061 Al alloy fixed at the advancing side. Condition B identified the opposite condition.

Friction stir welding has many welding parameters, such as tool (including shoulder and screw-like probe) materials, tool rotation speed, welding speed and the angle of the tool. In this study, only welding speed was considered and changed from 87 mm/min to 267 mm/min. Other parameters were fixed at 1600 rpm of the tool rotation speed and 3 degrees of the tool angle. The welding tool was rotated in the clockwise direction and parts, where the specimens were tightly fixed at the backing plate, were traveled.

Microstructural changes from the weld zone to the unaffected base metal were examined with OM (Optical Microscope), SEM (Scanning Electron Microscope) and TEM (Transmission Electron Microscope). The optical microstructure of the weld zone can be distinguished 6061Al from A356 Al alloy because each material showed the different etching response to the Keller etchant. For TEM observation, thin-foil disk specimens, 3 mm in diameter, were cut from various locations in the weld zone using the electron discharge machine and were prepared by twin-jet electro polishing in nitric acid/methanol solution at 243 K. This thin foils were observed at 300 kv using a JEOL transmission electron microscope. The composition of the precipitates and Si particles were analyzed by the TEM-EDS (Energy Dispersive Spectroscopy) analysis system.

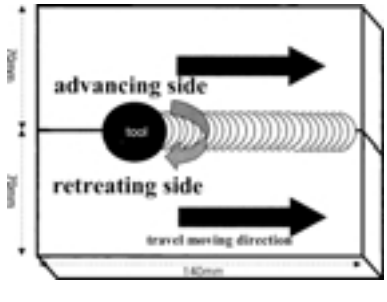

Figure 1 Schematic illustration of each weld side and welding process.

The Vickers hardness profile near the weld zone was measured on a cross section and perpendicular to the welding direction with a 100 gf load for 10 s. The tensile test was carried out at room temperature using an Instron-type testing machine with crosshead speed of 1.67×10^{-2} mm/s. To determine the tensile strength of the stir zone, tensile test specimens were sectioned in the longitudinal direction to the weld line by an EDM (electrical discharge machine).

3. Results and discussion

3.1. Microstructure evolution

Fig. 2 shows the surface appearances with the fixed location of each materials and welding speed. Regardless of welding conditions, any defects such as distortion, surface cracks and void, couldn't be observed on the upper and rear weld surfaces. From the observation of joints surface quality, FSW was applicable welding method and very wide range of welding conditions could be selected to join these dissimilar formed Al alloys. However, the width of weld bead had a small variation with welding conditions.

Fig. 3 represents the relation between the width of welding bead and welding speed with the fixed location of each material. The welding bead width slightly decreased with increasing welding speed because a lower welding speed resulted in a larger welding time and resultantly the weld zone received more plastic deformation.

The welding bead width for condition B (6061 fixed at retreating side) was wider than that for condition A (A356 fixed at retreating side). These results could be attributed to the difference resistance to the shear deformation during the welding process. The welding bead width ranged from 13.25 mm to 15.6 mm with each welding conditions.

Fig. 4 gives the variable macroimages of the cross-sectional weld zone with various welding conditions. From the different etching response of each material, 6061 Al alloys appeared as darker color than A356 Al alloys in the stir zone. For condition A, lighter color regions that were estimated as that of A356 Al alloys occupied larger fraction in the stir zone. However, for condition B, the microstructure of the stir zone was mainly composed of that of 6061 Al alloys. The macrostructure of the stir zone was mainly composed of the retreating side materials and some of the advancing side material.

The onion ring patterns were obviously observed in right part of the stir zone and characterized by the stacking of two materials. The area of the stir zone showed

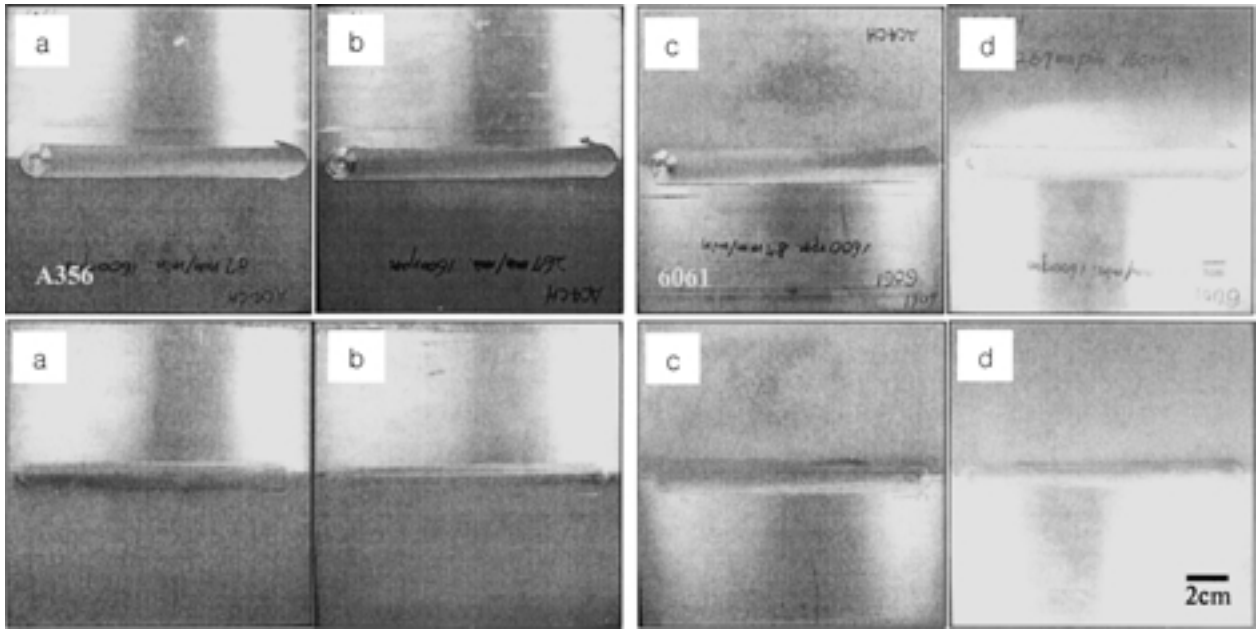

Figure 2 Photos of weld surface with various welding condition (upper: upper surface, below: rear surface): (a) 87 mm/min, (b) 187 mm/min: condition A, (c) 87 mm/min, and (d) 187 mm/min: condition B.

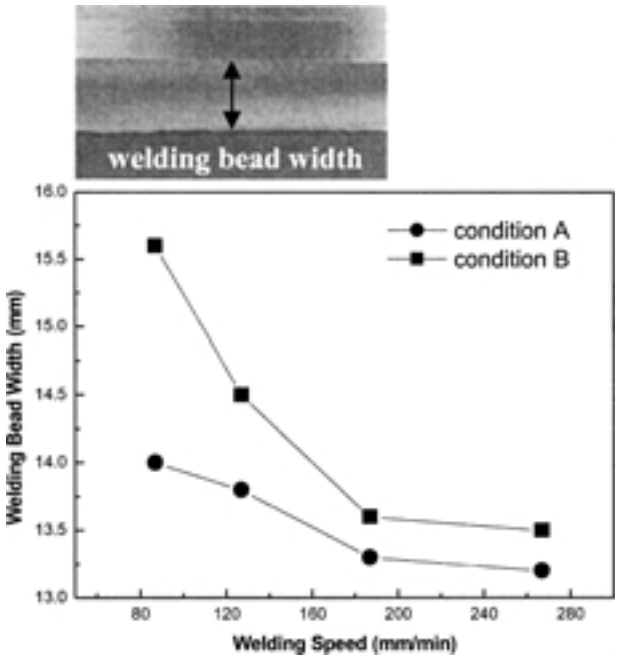

Figure 3 Variation of welding bead width with welding speed.

almost the same regardless of the fixed location of each material. However, the area of the stir zone slightly decreased as welding speed increased due to the different welding time and the cooling rate.

Fig. 5 shows the enlarged microstructures of the onion ring patterns with welding conditions. Onion ring patterns was characterized by the lamellar like structures stacked by the two materials. The homogeneously stacked two materials can be observed at lower welding speed. However, the difference width of the each two layers became larger with increasing welding speed.

Fig. 6 shows the microstructures of the base metals obtained by SEM and TEM. The dendrite microstructure of the A356 Al alloy was composed of primary α phase and Al-Si eutectic structure. The eutectic Si particles were partially distributed in the Al matrix. The 6061 Al alloy showed nearly equiaxed grain structure and the average grain size was about 15–20 μm. There were many etch pits which may be site of the second precipitate particles.

The 6061 base metal have two kinds of precipitates. Mainly observed one was Mg_2Si precipitates and the other was rarely observed AlFeSi precipitates. Mg_2Si precipitates were divided into fine needle-shape and rod-shape precipitate as their different morphologies. It has been already known that the main strengthening precipitate is fine needle precipitate because fine needle-shape precipitates are partially and completely coherent with the matrix and rod-shape shape precipitates have a low coherency with the matrix [20–22]. The size of fine needle-shape precipitates and the rod-shape precipitates were less 10 nm and about 50 nm long, respectively.

Fig. 7 shows TEM microstructures of A356 base metal and the stir zone for condition A. The dendrite microstructure of A356 alloys disappeared in the stir zone. The stir zone of this condition was composed of dispersed Si particles in the dynamic recrystallized microstructure. The eutectic Si particles were homogeneously distributed in the stir zone and their size were about 0.4–1 μm. The dynamic recrystallized grains characterized by fine and equaxied grain structure were formed by the plastic deformation and the simultaneously occurred frictional heat. Sub-grain and dislocation cell structure were also observed in the grains because severe plastic deformation was induced in the weld zone [23]. These structures gave the evidence that the recrystallization of stir zone during the friction stir welding process was produced by dynamic process [9].

Fig. 8 shows the TEM microstructures of 6061 base metal and the stir zone for condition B. Precipitates existed in the base metal disappeared in the stir zone. This result means that the temperature of the weld zone reached the resolving temperature of the precipitates.

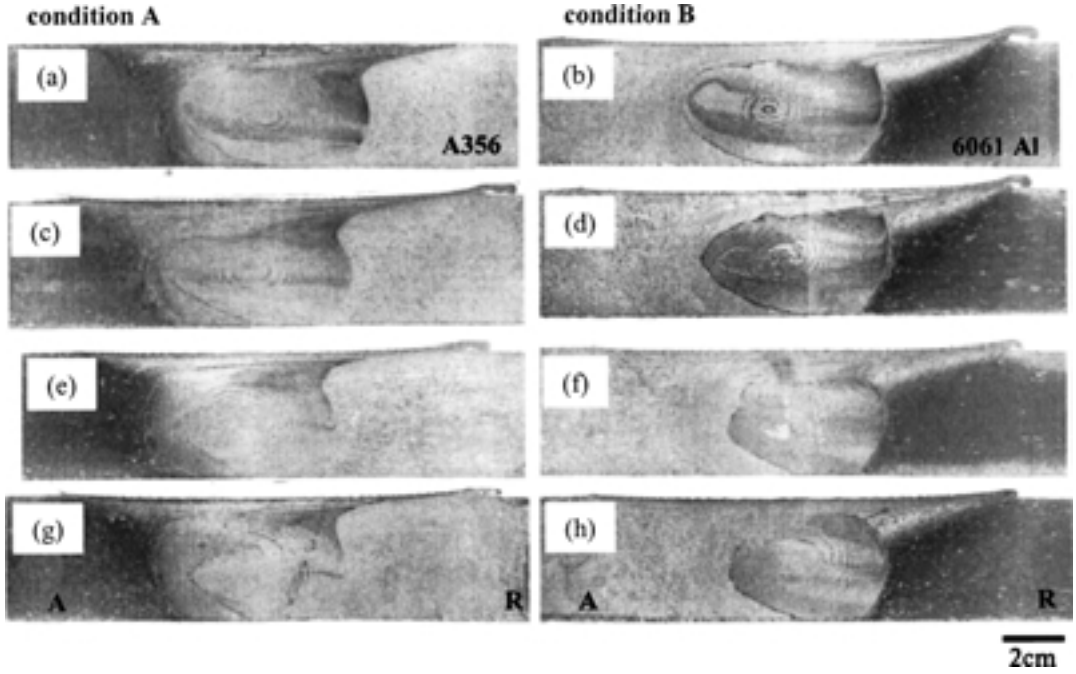

Figure 4 Macrostructure variation near the weld zone with various welding speed (a), (b): 87 mm/min, (c), (d):127 mm/min, (e), (f): 187 mm/min, (g), (h): 267 mm/min.

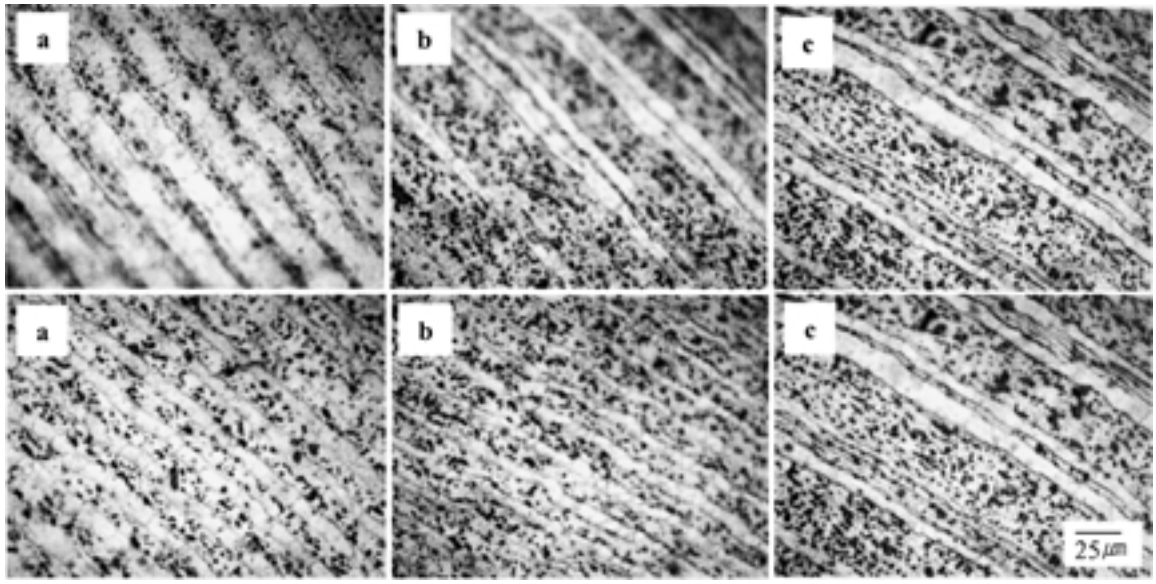

Figure 5 Microstructures of the enlarged onion ring pattern (upper: condition A, below: condition B): (a) 87 mm/min, (b) 187 mm/min, and (c) 267 mm/min.

The stir zone was mainly composed of the dynamic recrystallized grain structure and some of the rarely distributed Si particles. The sub-grain was also observed in the grains.

Fig. 9 represents the TEM micrographs of transition regions of 6061 and A356 side. Transition region of 6061 Al alloys had a high density of the rod-shape precipitates. The coarsened rod-shape precipitates grew into be a lager size, about 100–150 nm, by the welding heat. This result means that the temperature of transition region might reach a slightly lower temperature of the resolving temperature of precipitates and fine needle-shape precipitate almost disappeared in this region. Transition region of A356 Alloys was characterized by very long Si particles, the high density of sub-grain and the dislocation cell structure.

According to the previous report about the simulated weld thermal-cycle test [10], in the temperature range from 525 to 626 K, the density of needle-shape precipitates decreased and that of rod-shaped precipitates increased with increase temperature. The temperature higher than 675 K led the dissolution of all precipitates. The temperature of the stir zone and the transition region can be estimated over the 675 K and 626 K, respectively, from the observation of precipitate behaviors in weld zone using TEM.

3.2. Mechanical properties related to the microstructure

The relation between precipitates, Si particle distribution and hardness in the weld is summarized in Fig. 10.

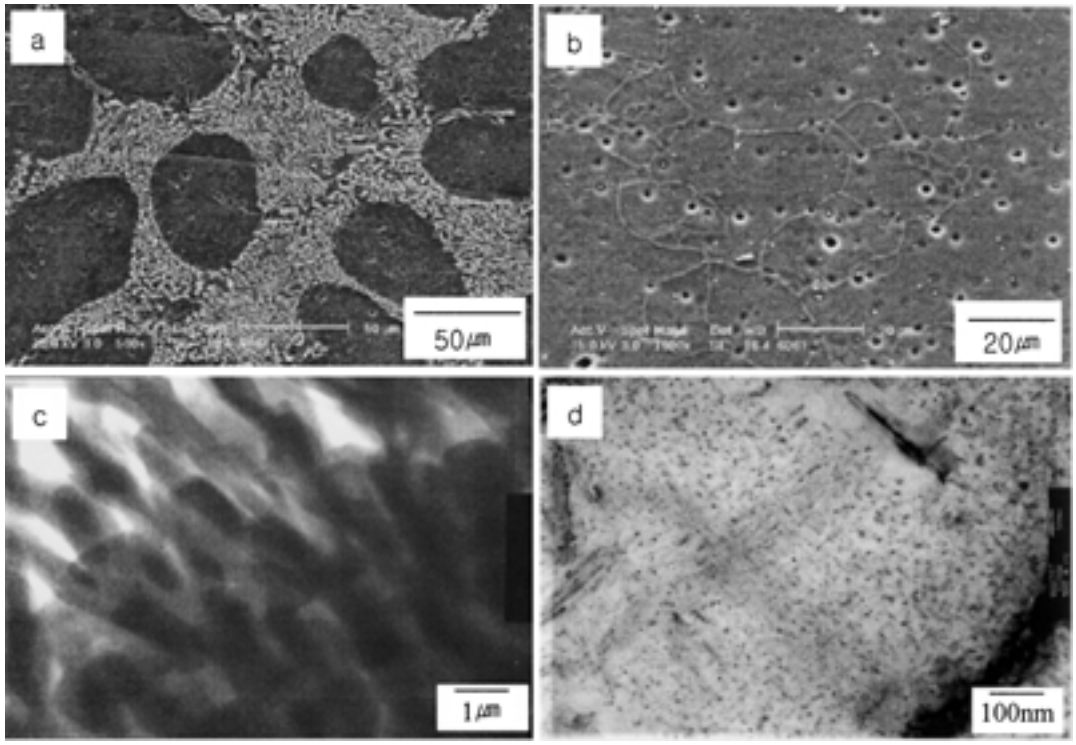

Figure 6 Microstructures of the base metal obtained by SEM (a, b) and TEM (c, d): (a, c) represent A356 and (b, d) represent 6061 Al alloy.

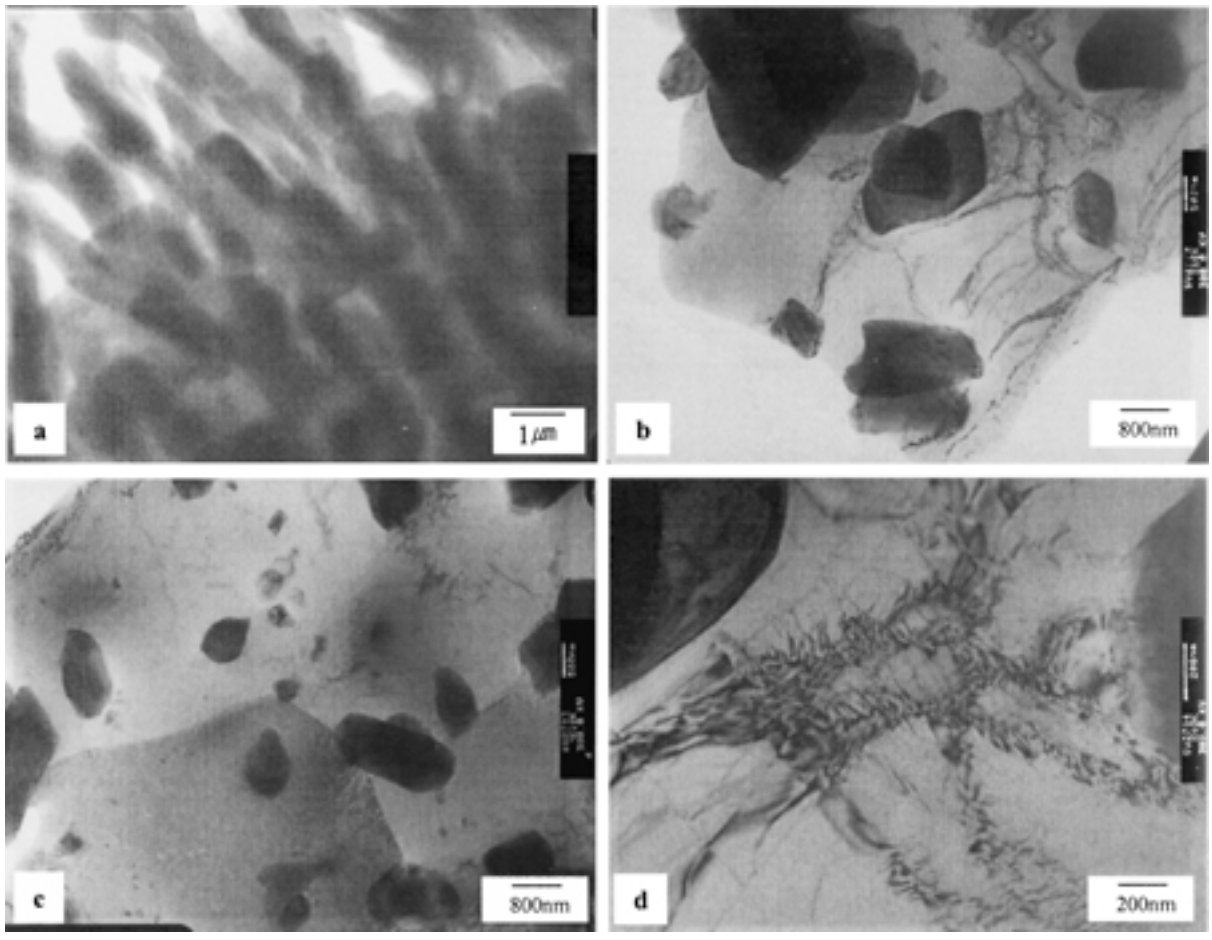

Figure 7 TEM micrograph of A356 base metal (a) and each part of stir zone (b–d) for condition A.

Fig. 10 indicates the cross-sectional hardness profile near the weld zone and related microstructure for condition B. Hardness of the stir zone was lower than that of 6061 Al alloy, but higher than that of A356 Al alloy. In a precipitation hardened Al alloy, the mechanical properties of the weld zone mainly depended on the precipitates behavior during the welding thermal cycles. From TEM observation of each region, Mg_2Si precipitates existed in the base metal with the morphology of fine needle and rod shape were dissolved in the stir zone.

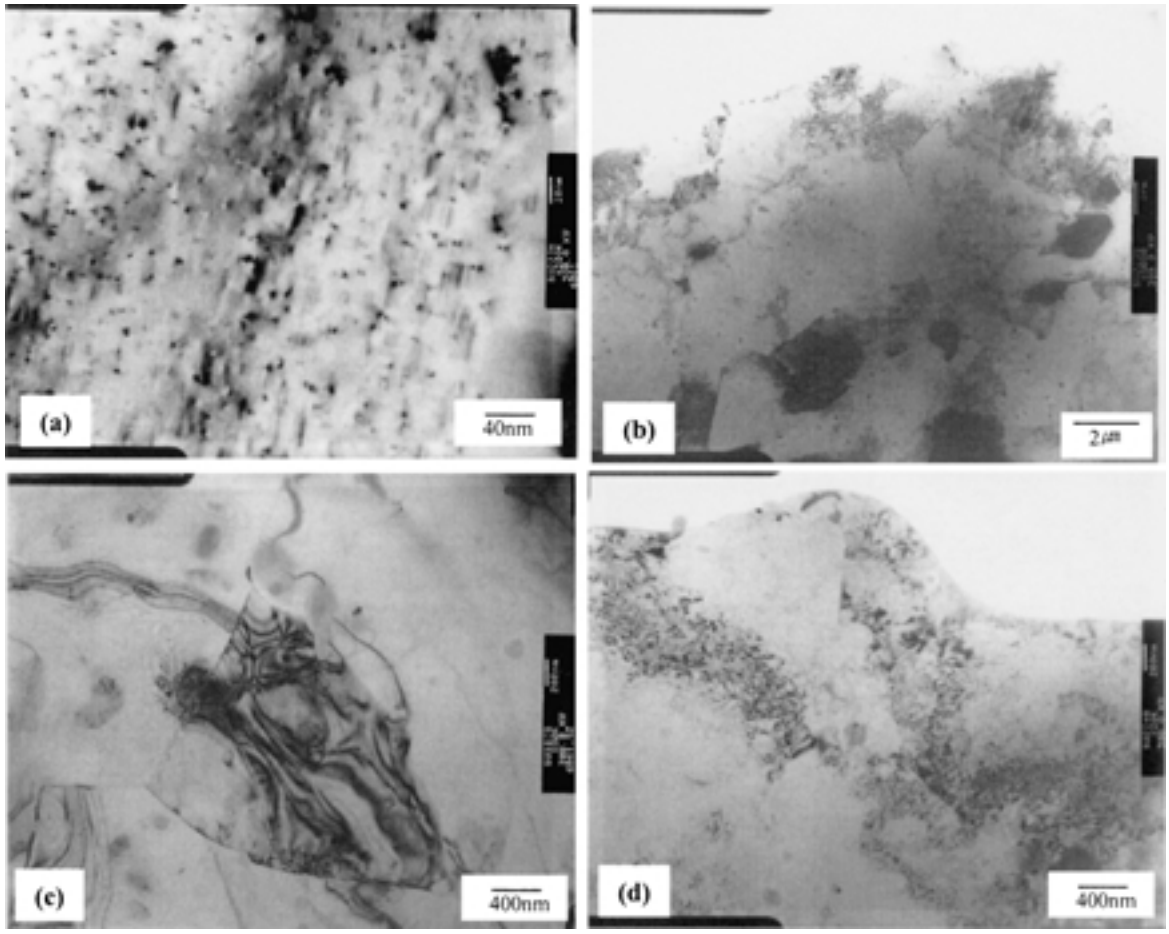

Figure 8 TEM micrographs of 6061 base metal (a) and each part of stir zone (b–d) for condition B.

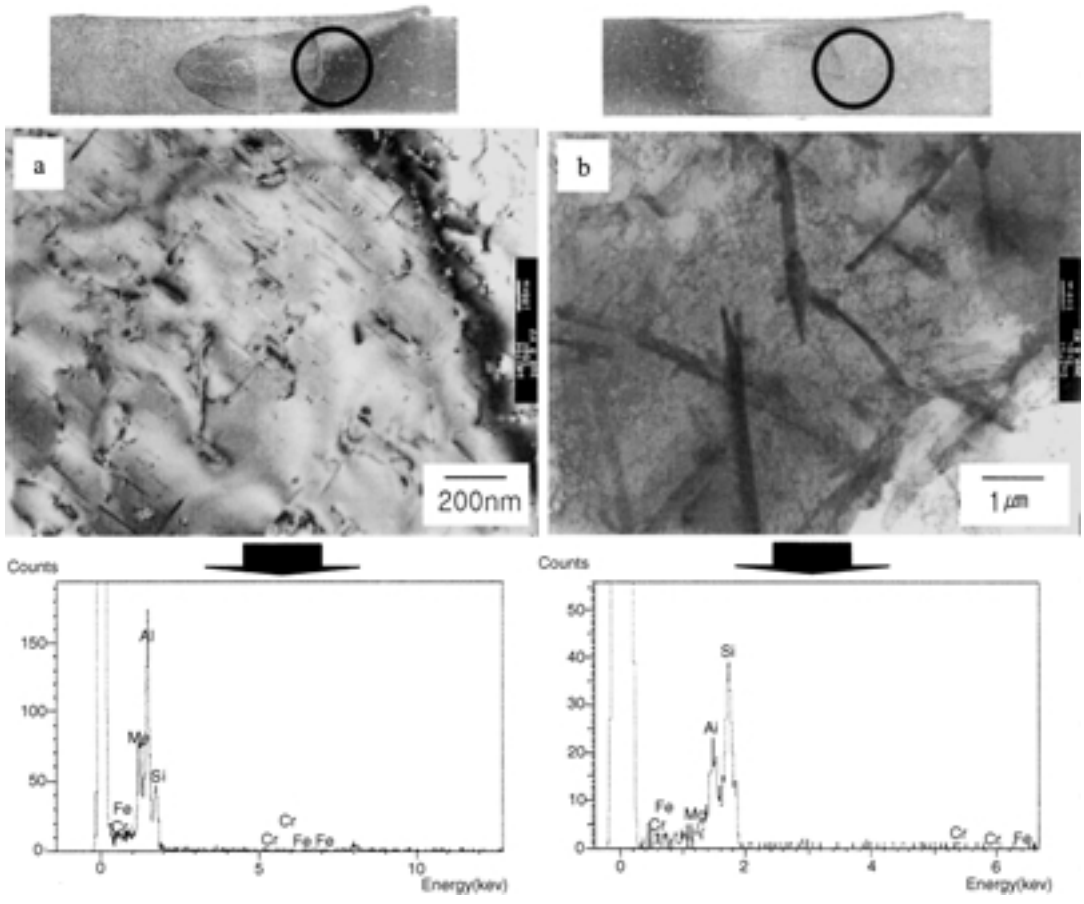

Figure 9 TEM micrographs and EDS results of transition region: (a) 6061 retreating side and (b) A356 retreating side.

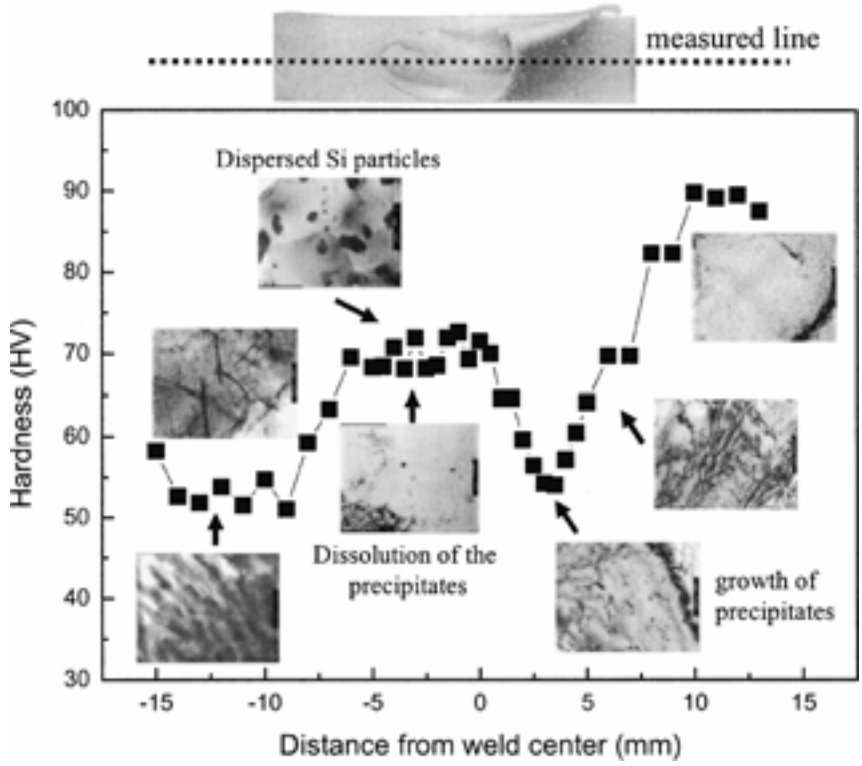

Figure 10 Relationship between the behaviors of precipitates, Si particles and hardness profile near the weld zone.

This result could be attributed to the reason why lower hardness than that of 6061 Al base metal. However, because eutectic Si particles of cast A356 Al alloy were homogeneously distributed in the stir zone, the stir zone showed a higher hardness than that of transition region which had a high density of rod shape precipitates.

Hardness of the stir zone showed higher values than that of A356 Al alloy base metal which had non-homogeneously distributed eutectic Si particles in Al solid solution matrix due to homogeneously dispersed Si particles and fine recrystallized grain structure.

Fig. 11 represents the hardness profile near the weld zone with various welding conditions. Hardness of the stir zone had a higher values if the 6061 Al alloy was located in the retreating side (condition B) because the microstructure of the stir zone was mainly dominated by the retreating side material. The difference of hardness in the stir zone was about 5–10 HV according to the fixed location of each material.

Hardness of the stir zone showed more scattered values at higher welding speed for condition A. According to our previous papers [24], a higher welding speed resulted in less homogeneously dispersed Si particles. Therefore, larger difference of hardness with hardness measured location was represented compared to that of lower welding speed conditions.

Hardness of the stir zone slightly increased as welding speed increases for condition B. This was mainly due to the different thermal effect with welding conditions. The thermal effect of FSW depended on the welding condition [25]. More thermal effects were added when the welding speed was slower and the tool rotation speed was higher, therefore the grain size and precipitates might grow at the lower welding condition.

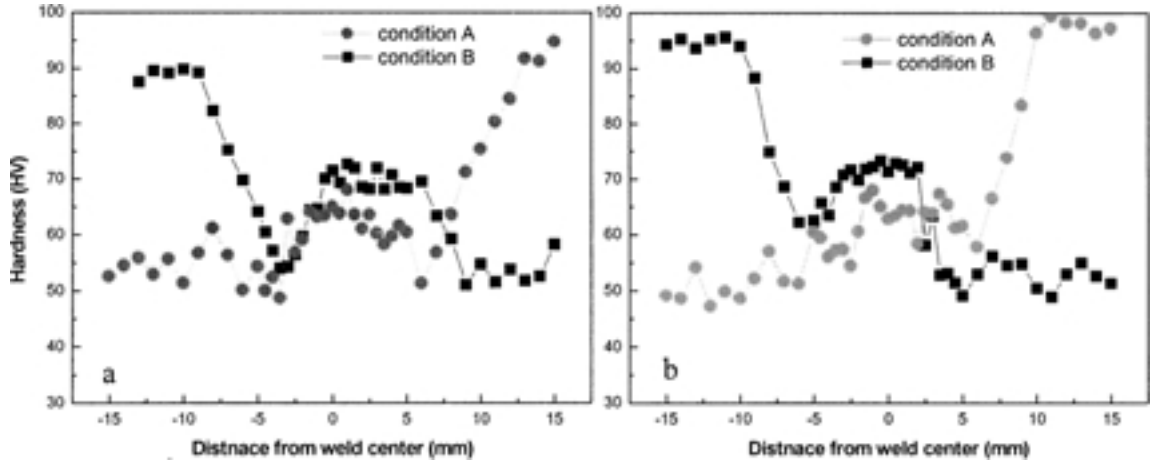

Figure 11 Hardness distribution near the weld zone with various weld conditions: (a) 87 mm/min and (b) 267 mm/min.

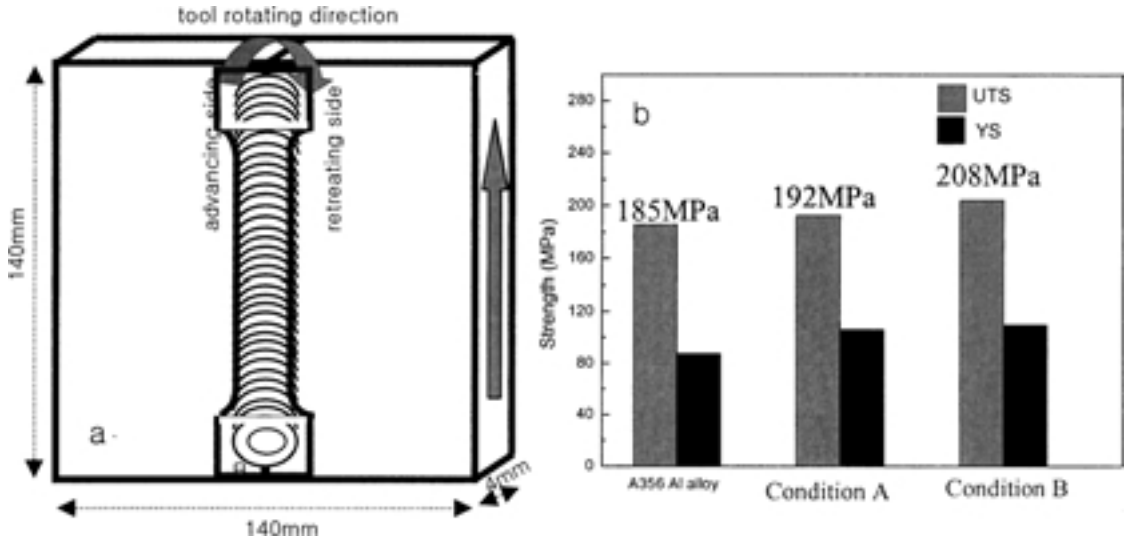

Figure 12 Shape of the longitudinal tensile test specimen (a) and longitudinal tensile strength (b).

The ultimate tensile strengths of base metals were 149 MPa for A356 Al alloy and 276 MPa for 6061 Al alloy, respectively. The transverse tensile strength of joints showed a same value compared to that of A 356 Al alloy regardless of welding conditions because fractures always occurred at the A356 Al alloy regardless of welding conditions. To evaluate only the strength of the weld zone, the longitudinal tensile specimens should be tested with various welding conditions and the results are shown in Fig. 12. The strength of the weld zone of similar A356 joint shows 185 MPa for UTS (ultimate tensile strength) and 87 MPa for YS (yield strength), which were higher strength than that of A356 Al alloy base metal [24]. The strength of the weld zone showed 192 MPa for UTS and 105 MPa for YS for condition A. The highest strength of the weld zone was acquired for condition B, which showed 208 MPa for UTS and 107 MPa of YS. The reason of the different strength according to the fixed location of each material was explained by the dominant microstructure in the stir zone.

4. Conclusion

Dissimilar formed Al alloys were joined using friction stir welding method and the main conclusions are as follow.

1. Defect free welding condition of friction stir welded dissimilar formed A356/6061 Al joints were acquired under wide range of welding conditions.

2. Microstructures of A356/6061Al joints showed mixed structures of two materials. The onion ring pattern, which appeared like lamellar structure, was observed both at the retreating side and the weld center.

3. Microstructure of the weld zone was composed of mainly fixed at the retreating side material and some of the advancing side material.

4. Hardness distribution near the weld zone was related to the microstructure of each region such as, precipitate, Si particles behavior and dislocation density. Hardness of the stir zone showed slightly lower than that of 6061Al base and was higher than that of A356 alloy base metal.

5. Transverse tensile strength of the joints showed a similar value with that of A356 base metal regardless of welding conditions. The longitudinal tensile strength of the stir zone showed the highest value in case harder material (6061Al) was fixed at the retreating side (condition B). These results can be attributed to the dominant material in the stir zone.

References

1. H. OKAMURA, K. AOBA and M. EZUMI, *J. Jpn. Inst. Light Met.* **50** (2000) 166.
2. S. KALLEE, D. RICHARDSON and I. HENDERSON, *Schweissen Schneiden (Welding cutting)* **36** (1997) 69.
3. M. R. JOHNSEN, *Weld. J.* **78** (1999) 35.
4. M. B. ELLIS and M. STRANGWOOD, *Mater. Sci. Technol.* **12** (1996) 970.
5. L. A. GUITTEREZ, G. NEYE and E. ZSCHECH, *Weld. J.* **75** (1996) 115s.
6. J. HAGSTROM and R. SANDSTROM, *Sci. Technol. Weld. Join.* **2** (1997) 199.
7. A. J. SUNWOO and J. W. MORRIS, Jr., *Weld. J.* **68** (1989) 262s.
8. C. J. DAWES and W. M. THOMAS, *ibid.* **75** (1996) 41.
9. Y. S. SATO, S. H. C. PARK and H. KOKAWA, *Metall. Mater. Trans.* **32A** (2001) 3033.
10. Y. S. SATO, H. KOKAWA, M. ENOMOTO and S. JORGAN, *ibid.* **30A** (1999) 2429.
11. G. LIU, L. E. MURR, C.-S. NIOU, J. C. McCLURE and F. R. VEGA, *Scripta Mater.* **37** (1997) 355.
12. L. E. MURR, G. LIU and J. C. McCLURE, *J. Mater. Sci.* **33** (1998) 1243.
13. K. N. KRISHNAN, *Mater. Sci. Eng.* **A327** (2002) 246.
14. T. U. SEIDEL and A. P. REYNOLDS, *Metall. Mater. Trans.* **32A** (2001) 2879.
15. Ø. FRIGAARD, Ø. GRONG and O. T. MIDLING, *ibid.* **32A** (2001) 1189.
16. P. ULYSSE, *Int. J. Mach. Tool Manu.* **42** (2002) 1549.
17. Y. LI, L. E. MURR and J. C. McCLURE, *Mater. Sci. Eng.* **A271** (1999) 213.
18. L. E. MURR, Y. LI, R. D. FLORES, E. A. TRILLO and J. C. McCLURE, *Mater. Res. Innov.* **2** (1998) 150.
19. S. TANAKA and M. KUMAGAI, in Proceedings of the Third International Symposium on Friction Stir Welding, Kobe, Japan, Sept. 2001, p. 27.
20. D. L. ZHANG and L. ZHENG, *Metall. Mater. Trnas.* **27A** (1996) 3983.

21. M. H. JACOBS, *Phil. Mag.* **26** (1972) 1.
22. I. DUTTA and S. M. ALLEN, *J. Mater. Sci. Lett.* **10** (1991) 323.
23. K. V. JATA and S. L. SEMIATIN, *Scripta Mater.* **43** (2001) 743.
24. W. B. LEE, Y. M. YEON and S. B. JUNG, *Mater. Sci. Eng. A* **355** (2003) 154.
25. Ø. FRIGAARD, Ø. GRONG and O. T. MIDLING, in Proceeding of INALCO'98, Cambridge, UK, 1998, p. 197.

Received 27 March
and accepted 22 July 2003